Subcontract NP-1

WANL-TME-1708
November 1967

Westinghouse Astronuclear Laboratory

WESTINGHOUSE ASTRONUCLEAR LABORATORY CONTRIBUTION TO THE TWENTY-FIFTH HIGH TEMPERATURE FUELS COMMITTEE MEETING DECEMBER 5, 6, AND 7, 1967

(Title Unclassified)

DISCLAIMER

~~CONFIDENTIAL~~
~~RESTRICTED DATA~~
Atomic Energy Act - 1954

MASTER

Subcontract NP-1

WANL-TME-1708
November 1967

Westinghouse Astronuclear Laboratory

WESTINGHOUSE ASTRONUCLEAR LABORATORY CONTRIBUTION TO THE TWENTY-FIFTH HIGH TEMPERATURE FUELS COMMITTEE MEETING DECEMBER 5, 6, AND 7, 1967

(Title Unclassified)

DISTRIBUTION OF THIS DOCUMENT UNLIMITED

Edited by:
L. R. Fleischer

GROUP - 1
EXCLUDED FROM AUTOMATIC DOWNGRADING AND DECLASSIFICATION

INFORMATION CATEGORY
C. R. D.
J. M. Dingley 11/28/67
AUTHORIZED CLASSIFIER DATE

SPECIAL REREVIEW FINAL DETERMINATION
Reviewer TR Class. 4 Date 5-6-82
Class: 4

(The preliminary information presented in this report should not be published without prior written approval of the Westinghouse Astronuclear Laboratory. The work performed was supported by the Space Nuclear Propulsion Office).

~~CONFIDENTIAL~~
~~RESTRICTED DATA~~
Atomic Energy Act - 1954

Classification cancelled (or changed to _____
by authority of TID-1401-52
by [illegible] DTIE, date 7-14-75

PAGE BLANK

Astronuclear Laboratory

TABLE OF CONTENTS

PAGE BLANK

LIST OF ILLUSTRATIONS

LIST OF ILLUSTRATIONS (CONTINUED)

LIST OF TABLES

1.0 INTRODUCTION

(U) The nuclear rocket program currently employs two types of operational testing. In one series, designated NRX-, reactor design and materials performance are tested in terms of power production, temperature capability and longevity. The other series of tests, designated XE-, are rocket engine systems tests, aiding in the development of engine components.

(U) The first engine component test was combined with the fourth of the NERVA reactor tests, called NRX-EST. In this experiment the system was started and operated without the use of an external power supply for propellant pumping. This established the capability of the system to generate auxiliary power for pumping and control functions in addition to propulsion power. The subsequent tests in the series, XE-1 and XE-2, are aimed at further development of the liquid hydrogen subsystem in a flight-oriented configuration.

(C) NRX- and XE- reactors are structurally similar. Fuel elements are clustered around unfueled elements containing a tie rod. A support block at the downstream end of the fuel cluster is connected to an upper support plate at the inlet end, supporting the fuel axially. The fuel clusters are bundled together to form the core by a spring loaded lateral support system.

(C) The fuel elements are a dispersion of pyrocarbon-coated UC_2 particles in a graphite matrix. They are extruded with a hexagonal cross section and nineteen full length, longitudinal coolant channels. The coolant channels and other surfaces exposed to a corrosive hydrogen environment are protected with a vapor deposited coating. The fuel for the first five NRX- reactors was coated with NbC, deposited at temperatures on the order of 1900°C. Because of the differences in the thermal expansion rates of NbC and the graphite base fuel, the coating cracked on cooling. These cracks remained open at reactor operating temperatures below the coating deposition temperature. As described at the Twenty-Fourth Meeting of the High Temperature Fuels Committee (WANL-TME-1611), laboratory tests and a limited number of experimental fuel elements in reactor tests indicated improved corrosion resistance of elements with Mo vapor deposited at low temperature, closing the cracks in the NbC (now deposited at about 1600°C).

(U) This report describes the electrically powered corrosion test used for the development and qualification of fuel for the NRX-A6 reactor. This reactor is currently at the Nevada Test Site and will be tested in the near future. Also, an old problem which recurred when the XE-1 reactor was shipped to the test site, causing postponement of the test, is discussed.

(U) The axial support structures of the reactors are subjected to the same rigorous environment as the fuel. Therefore, the materials problems encountered by these structures are of interest to the Fuel Development Department. A group within the Fuel Development organization is concerned with the manufacture and testing of support blocks and the development of high temperature materials to improve the performance of these components. Some of this work is reported in the last two sections of this document.

2.0 CORROSION PERFORMANCE OF NRX-A6 FUEL ELEMENTS*

2.1 FUEL ELEMENT DESCRIPTION

(C) Graphite-base NRX-A6 fuel elements are protected against reaction with hydrogen coolant by a base layer of vapor deposited niobium carbide and a complementary molybdenum coating. Typical profiles of coating thickness as a function of position along the length of the fuel elements are shown in Figure 2-1. Cracks form in the base NbC coating as a result of the differences in the thermal expansion between the fueled graphite substrate and the NbC. The Mo coating is used to fill the cracks in the NbC, thereby forming a continuous protective coating over the coolant channel.

(C) Without the Mo coating, the cracks in the NbC in those regions of the fuel element operating below the NbC deposition temperature (1600°C), i.e., between 0 and 30 inches from the inlet end, would remain open. Excessive corrosion would occur in these regions because of the cracks. Coatings characterized by less than about 20 cracks/inch are generally lacking in adherence between the coating and the substrate. In such cases the molybdenum may not be entirely effective, and the corrosion rate is not decreased adequately. However, the NRX-A6 fuel elements have NbC coatings with 60 to 80 cracks/inch in the region of interest as shown in Figure 2-2. A greater than sixfold decrease in corrosion in the 0 to 35 inch region is realized with the addition of the molybdenum coating. This is shown graphically in Figure 2-3.

(C) In addition to the standard element described above, the NRX-A6 reactor also contains some elements which are variations of the standard. The elements placed at the periphery of the core were produced with a coating of NbC on the outer surfaces to protect against corrosion by hydrogen that may leak through the lateral support system. Other elements, designated as experimental elements, had niobium added to the matrix as 2.5 or 5.0 volume percent NbC additions or as a niobium resinate impregnant to evaluate advanced fuel concepts.

---

*R. A. Leasure

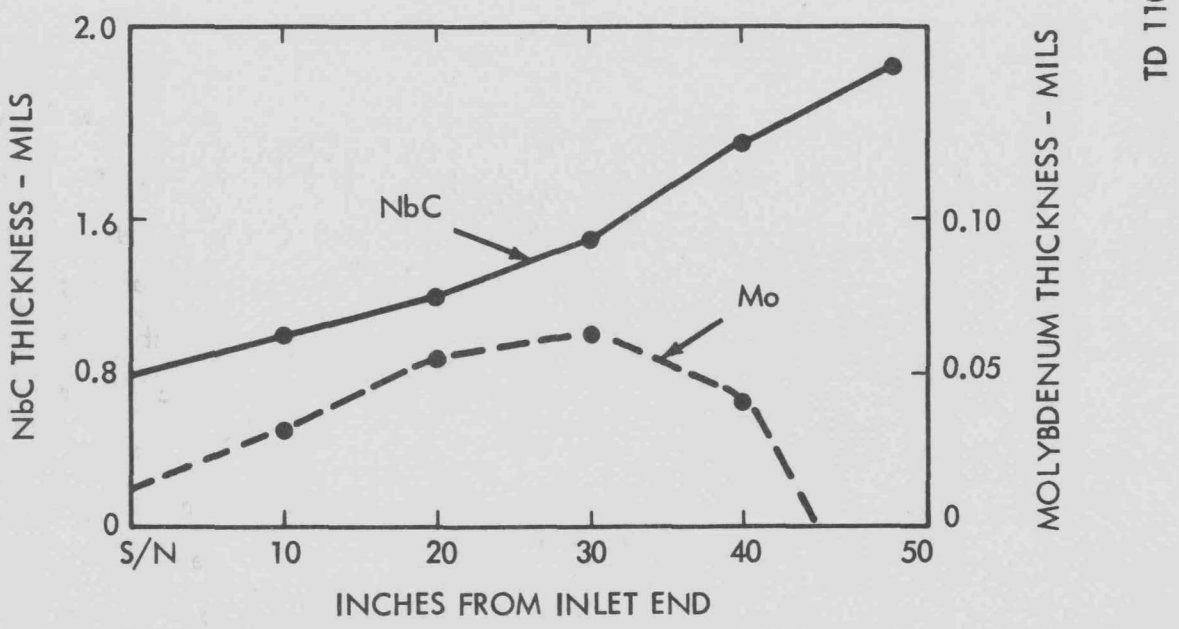

Figure 2-1.(C) Typical Coating Thickness Versus Position Profiles for NRX-A6 Fuel Elements(U)

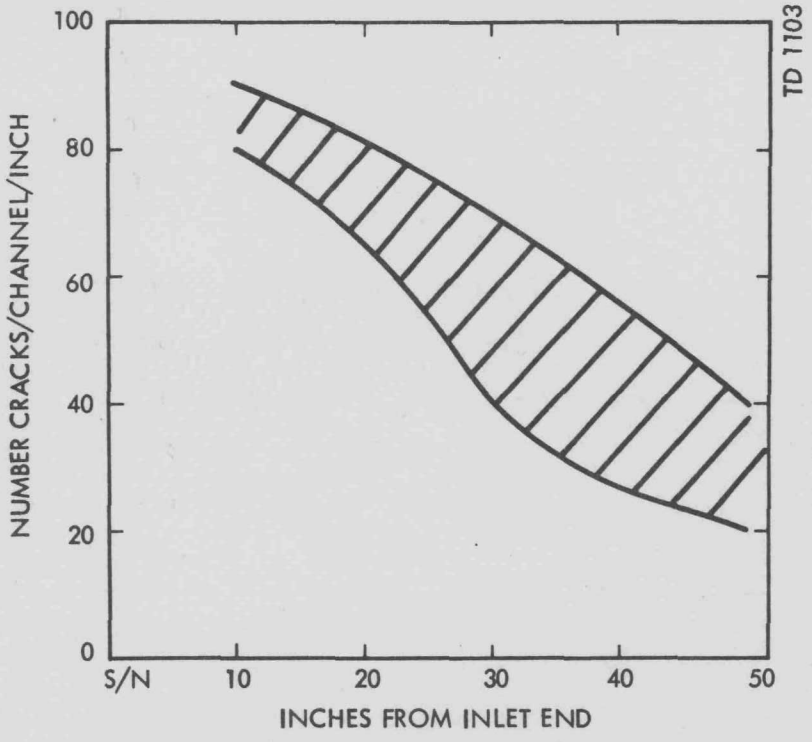

Figure 2-2.(C) Range of Crack Densities Observed in NbC Coatings on NRX-A6 Fuel Elements(U)

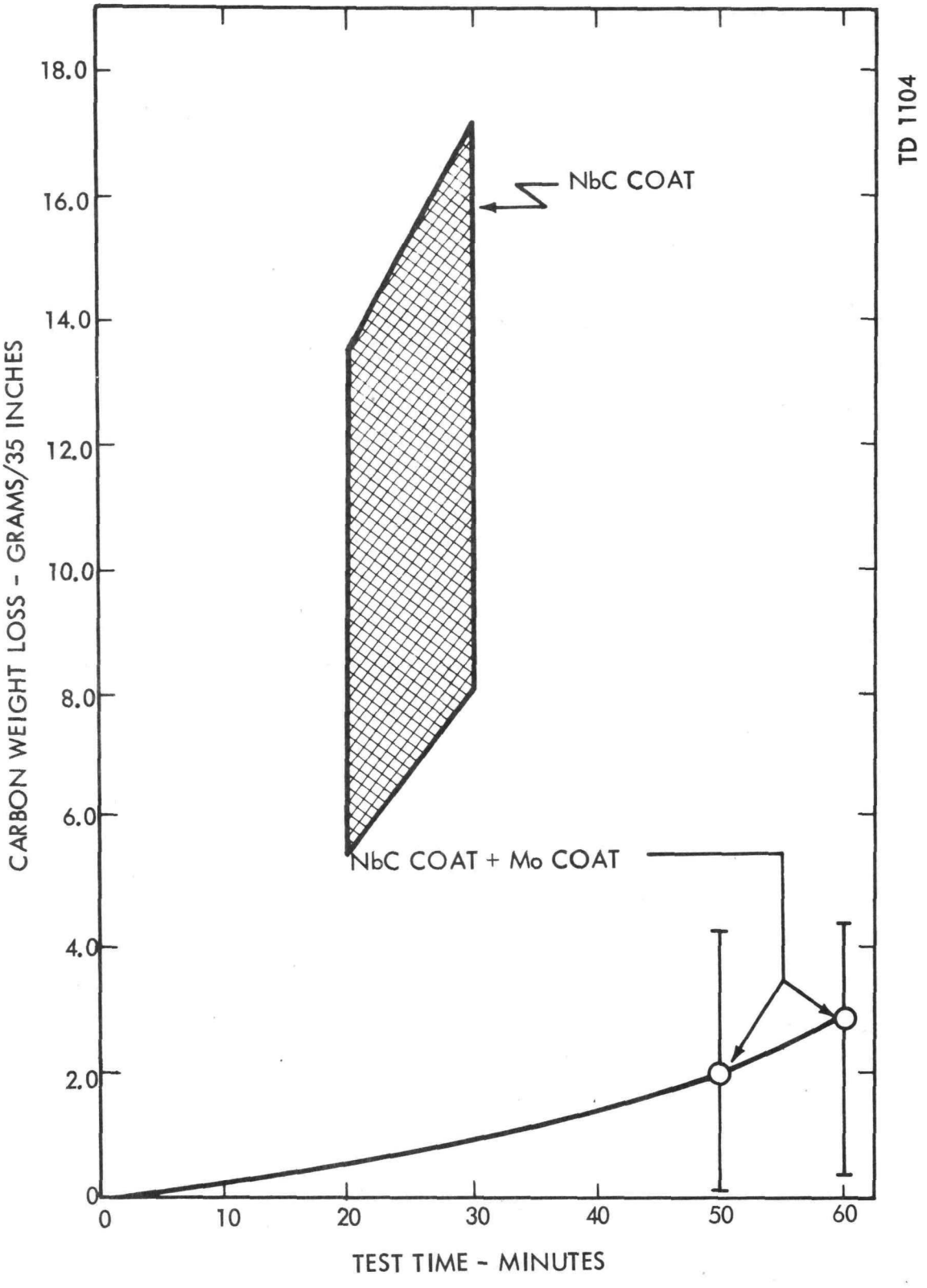

Figure 2-3. (C) Mid-Band Corrosion Weight Loss Versus Test Time for NbC Coated and for NbC + Mo Coated Fuel Elements (C)

2.2 CORROSION BEHAVIOR OF NRX-A6 FUEL ELEMENTS

2.2.1 Qualification Test - Description and Results

(C) The corrosion performance characteristics of the NRX-A6 elements were determined through an electrical powered hydrogen corrosion test. The test is designed to approximate the maximum power generation and flow conditions that would be experienced in the reactor by an element with a "hot channel." The electrical test consists of passing current (~ 4,000 amperes) through the full length of the element which is supported by graphite chuck-electrodes and flowing hydrogen (592 SCFM) through the coolant channels for 60 minutes in two 30-minute cycles. The nominal parameters for this test, which is designated as a PB 30 + 30 test, are shown in Figure 2-4 with the acceptance limits and a typical surface temperature profile. The maximum materials temperature is approximately 200°C higher than the surface temperature at Station 49.

(C) This test was evolved from electrical corrosion tests on NRX-A6 and NRX-A5 elements and comparison of these results with reactor behavior. The results show the same relative performance for the -A4 and -A5 elements when compared to reactor behavior and the test is expected to give results similar to the NRX-A6 reactor except for the hot end (Stations 35-52) behavior. Due to differences in average materials temperatures in this region for electrical and reactor tests, the hot end weight loss is expected to be lower in the reactor test by a factor of two.

(C) Fuel elements produced for use in NRX-A6 passed the acceptance limits given in Figure 2-4, i.e., time - 30 + 30 minutes, carbon weight loss - 20.0 grams, and surface - 75 percent and < 5 pinholes, with few exceptions. Typical weight losses experienced by the three general types of elements in NRX-A6 (standard, bore-OD, and experimental) are shown in Figure 2-5 with curves showing the typical weight loss distribution for standard elements and bore-OD-elements. Because of the added protection afforded by the molybdenum coating, the corrosion in the midband region (Stations 10-35) has been reduced from an average of 11 grams to about 2 grams (refer to Figure 2-3), which accounts for about 20 percent of the total weight loss in a corrosion test of an NRX-A6 element. The corrosion in the hot end region accounts for the remaining 80 percent or about 10 grams. (This is expected to be about 5 grams in the reactor.)

TEST CONDITIONS:

POWER GENERATION	900 KW
H_2 FLOW	592 SCFM
EXIT PRESSURE	560 PSIG
TIME	30 + 30 MINUTES

ACCEPTANCE LIMITS:

CARBON WEIGHT LOSS	< 20.0 GRAMS
END SURFACE REMAINING	75 %
PINHOLES	5 MAX.

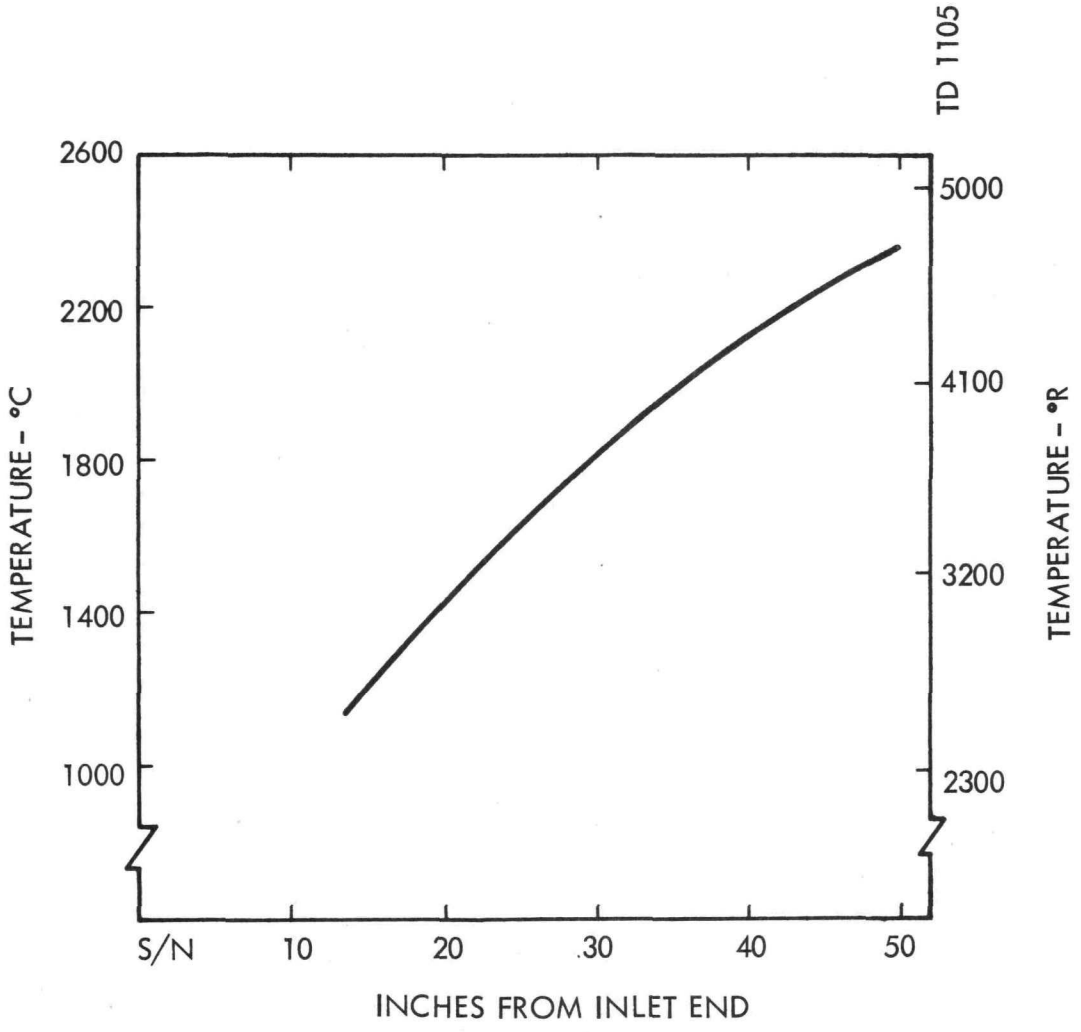

Figure 2-4. (C) Temperature Distribution, Test Conditions, and Acceptance Limits for NRX-A6 Fuel Element Qualification Corrosion Tests (U)

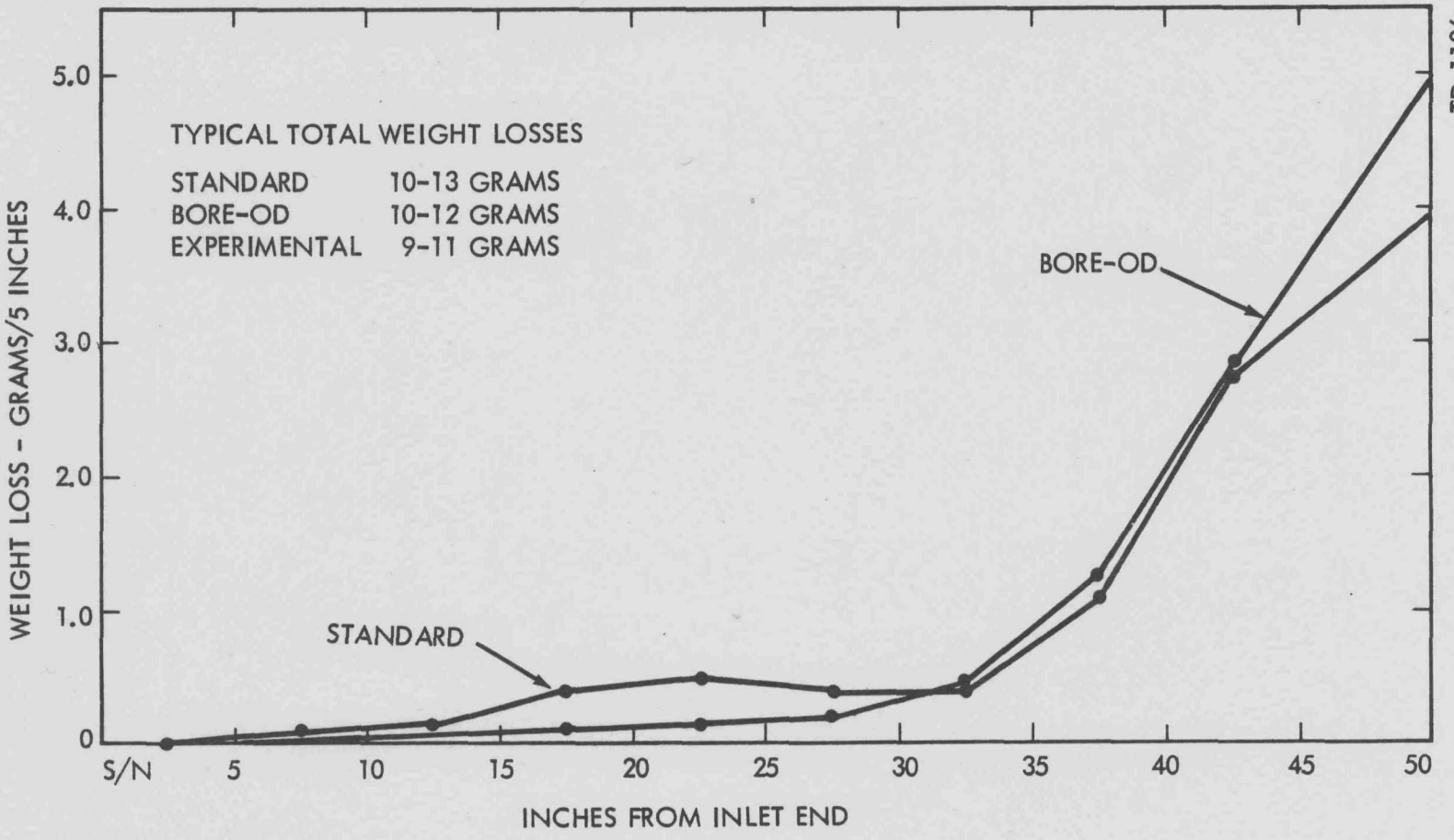

Figure 2-5. (C) Typical Weight Loss Distributions for NRX-A6 Standard Fuel Elements and Bore + OD Coated Fuel Elements (C)

(C) Differences noted between the weight loss distribution of the standard and bore-OD elements are probably due to slight differences in coating adherence and resultant crack density in the midband region. Because of the dependence of the hot-end corrosion on the carbon content of the hydrogen as a result of upstream corrosion, the bore-OD elements which have lower midband weight losses show hot end (Stations 35-52) weight losses slightly higher than the standard elements.

(U) Pinholes, which are defined as local corrosion pockets extending from the coolant channel to an outer surface, were minimal in the electrical corrosion tests.

2.2.2 Description of Corrosion Observed in NRX-A6 Elements

(C) The corrosion that is observed in the NRX-A6 fuel elements during the electrical corrosion test can best be described in relation to the region of the element in which it occurs. The corrosion which occurs in the midband region (Stations 10-35) is minimal owing to the protection provided by the molybdenum and NbC coating. The corrosion that does occur can be described as a selective corrosion of the binder carbon in the fuel matrix. The small amount of corrosion appears to originate from small cracks in the coating that are induced in handling prior to the corrosion test.

(C) The second area of corrosion is the hot-end region (Stations 35-52) which accounts for 80 percent of the total weight loss. The corrosion in this region is primarily diffusion controlled and starts as a selective attack of the binder carbon which becomes progressively more severe as the temperature increases with axial position. The more severe form of the hot end corrosion results in local corrosion pockets, generally located downstream of Station 45. In addition to the corrosion in this region, the high temperatures causes migration of the uranium carbide which is distributed throughout the matrix. Typical examples of the corrosion observed at 100X in the NRX-A6 elements as a result of the electrical corrosion test are shown in Figures 2-6A and 2-6B.

A) STATION 20, 100X

B) STATION 45, 100X

Figure 2-6. (C) Typical Corrosion in NRX-A6 Fuel Elements after PB 30 + 30 Corrosion Test, 100X (C)

3.0 XE-1 DEBRIS PROBLEM*

3.1 INTRODUCTION

(C) In late August of 1967, a significant problem was identified which generated a major reevaluation of activities related to NERVA fuel element hydrolysis. The specific problem was revealed by the presence of approximately 45 grams of fuel element debris in the XE-1 reactor which triggered an intensive laboratory problem to identify the cause and effect relationships. A 2-month program led to the October 1967 conclusion that hydrolysis of exposed UC_2 caused the observed debris. A summary of this investigation is the subject of this section.

(C) The XE-1 reactor is one of a series of graphite matrix nuclear reactors which is essentially identical to the NRX-A2 through -A5 reactors. The fuel elements used in the XE-1 consist of both Y-12 and Westinghouse produced -A4, -A5, and -A6 fuel elements produced before the addition of Mo coatings was adopted. The fuel element bores are coated with niobium carbide deposited at temperatures between 1800 and 1900°C. The coatings produced by this process are relatively non-adherent as compared to current production practice on the NRX-A6 and XE-2 reactors.

(C) The XE-1 reactor was completely assembled in early April 1967. The reactor was inerted with 8 psig helium and shipped to the Nevada Test Site in mid-April. The reactor remained in a sealed inerted condition until mid-August, at which time the reactor was opened to the atmosphere and the fuel element debris found.

3.2 CHARACTERIZATION OF XE-1 DEBRIS

(C) Samples of the XE-1 debris were submitted for metallographic, chemical, and particle size analysis. Figures 3-1 and 3-2 reveal low magnification and high magnification views of the XE-1 debris. The metallographic data clearly show that the major fraction of the debris consists of niobium carbide and that segments of the niobium carbide have a radius of curvature identical to that of the 100-mil diameter fuel element channels. The debris also shows a significant amount of uranium which, for the most part, appears to be a product of the hydrolysis reaction.

---

*A. Boltax

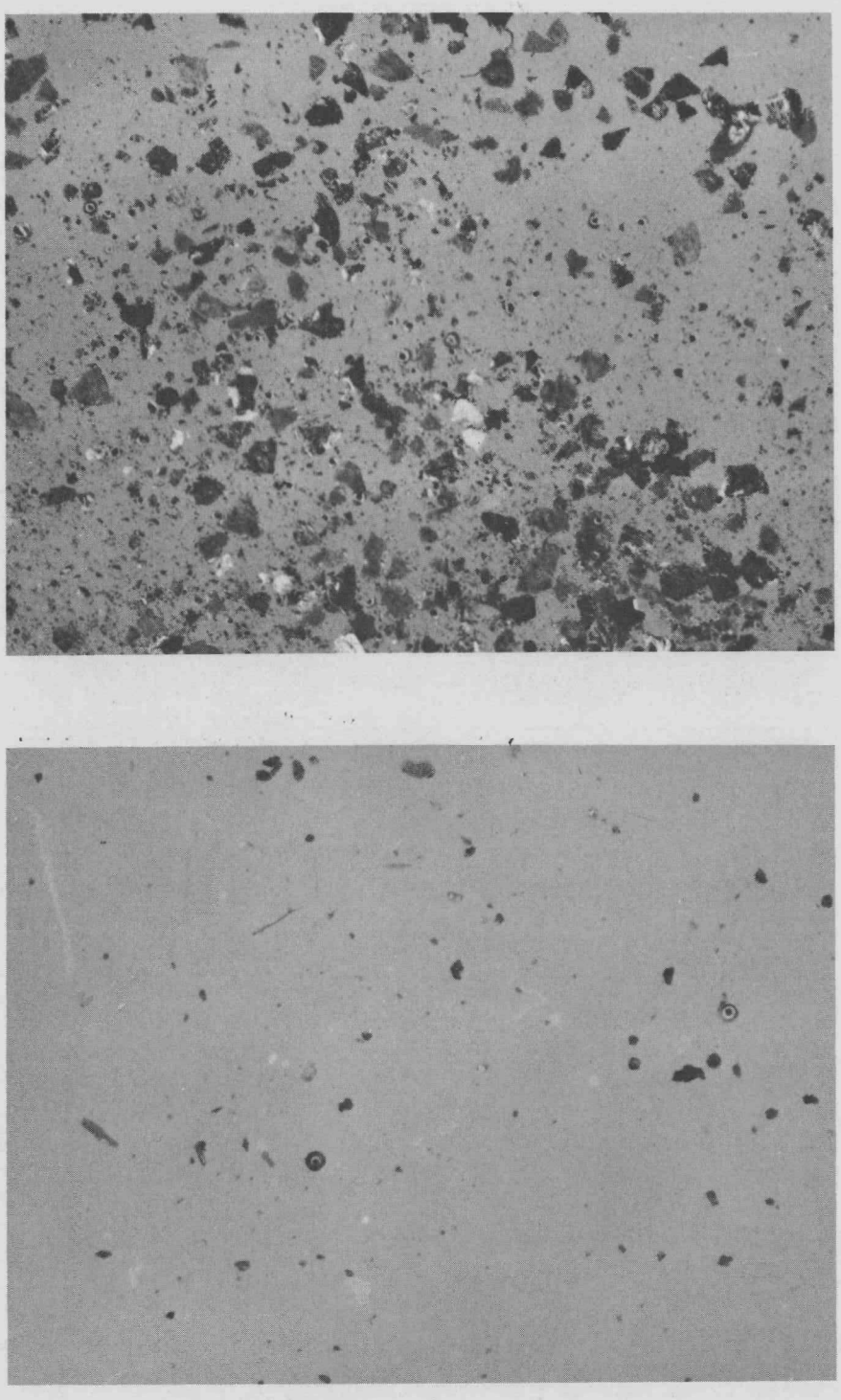

Figure 3-1 (C) Debris from XE-1 Fuel Elements, 20X(C)

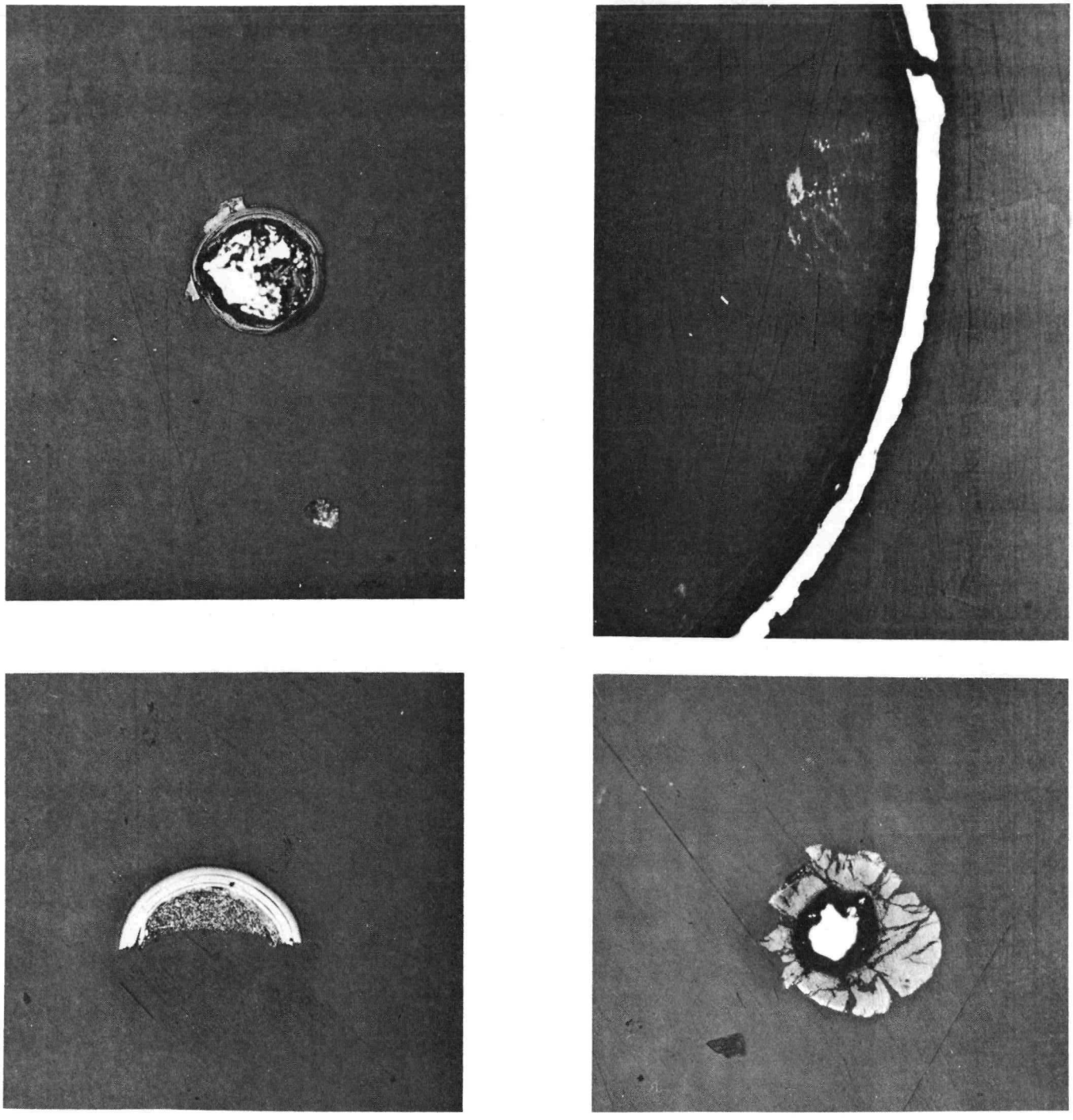

Figure 3-2. (C) Debris from XE-1 Fuel Elements, 200X. The Debris Contains Coated Fuel Particles (Small Quantity), Segments of NbC Bore Coating (Major Constituent), Pyrocarbon Shells(Small Quantity), and Hydrolyzed UC_2 Particles and Fragments(Significant Quantity). (C)

(C) Chemical analysis and particle size measurements are summarized in Table 3-1. The data indicate that the debris is approximately 84 percent niobium carbide and 13 percent uranium, with the balance identified as free carbon. Examination of the particle size data shows that the XE-1 debris is 99.6 percent less than 20 mils in size with 79 percent falling between 3 and 20 mils and 20 percent less than 3 mils in size. The data indicate that the uranium present consists mainly of particles less than 3 mils in diameter as compared to the original UC_2 bead size of 4 to 6 mils. The latter observation indicates the occurrence of a chemical reaction within the UC_2 particles.

(C) Examination of the XE-1 debris led to the tentative hypothesis that a hydrolysis reaction was responsible for producing the debris. An extensive laboratory investigation was initiated to evaluate this hypothesis.

3.3 REQUIREMENTS FOR HYDROLYSIS REACTION IN NERVA FUEL ELEMENTS

(U) The hydrolysis reaction in NERVA Fuel elements can be schematically represented by the following equation:

$$UC_2 + x\ H_2O \rightarrow UO_2 \cdot n\ H_2O + g\ H_2 + z\ C_kH_m,$$

where $UO_2 \cdot n\ H_2O$ refere to a hydrous uranium oxide and C_kH_m to a mixture of 30 or more hydrocarbons and water-insoluable wax. The reaction proceeds rapidly at ambient conditions with both water vapor and liquid water. Kinetic studies on UC_2 hydrolysis by water vapor indicate reaction rates of 0.044, 0.66, and 3.2 micrograms per centimeter square per second at 50, 150, and 200°C, respectively. Thus, the requirements for the hydrolysis reaction are apparent from the preceding discussion, i.e., exposed UC_2, water, and time.

(C) The major sources of exposed UC_2 in NERVA fuel elements arise from incomplete leaching of pyrocarbon-coated UC_2 particles cut by machining and UC_2 exposure due to carbon removal in a diffusion controlled NbC coating process. However, these sources of exposed UC_2 might not be subject to hydrolysis if the NbC coating did not allow an access of the external atmosphere through cracks in the coating and gaps between the coating and matrix. Examples of atmospheric accessability to exposed UC_2 in fuel elements are shown in Figure 3-3.

TABLE 3-1
(C) SUMMARY OF DATA ON XE-1 DEBRIS (C)

Sample No.	Sample Weight, gm.	Chemical Analysis	Radioactivity, dpm/g	Density, gm/cc	Remarks
1	3.7	U - 12.5% NbC - 85.5% C - 4.1%	---	---	99.7% coarser than 5 microns. Sample screened on 74 micron sieve.
1 - Coarse Fraction	2.9 (79.1%)	U - 1.87 to 3.81% NbC - 96.8 to 97.6% C ~ 1%	4.8×10^4	8.32*	Coarse fraction retained on 74 micron sieve.
1 - Fine Fraction	0.8 (20.9%)	U - 28.9 to 30.6% Nbc - 48.6 to 55.9% C ~ 20%	1.3×10^6	5.45	Fine fraction passed through 74 micron sieve
2	5.0	U - 13.6% NbC - 82.1% C - 4.3%	2.6×10^4	8.38*	Spark spectrometer shows presence of chloride ion contamination. 98.4% coarser than 5 microns.
3	14.86	---	---	---	99.6% finer than 20 mils.

*NbC density varies between 8 to 8.44 gms/cc

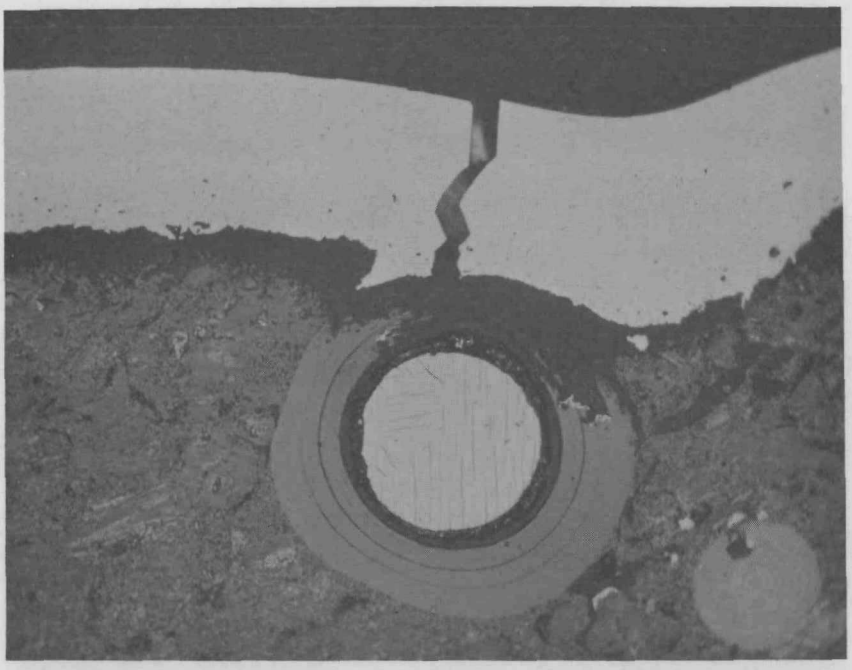

Figure 3-3A. (C) XE-1 Fuel Element Coating Is Generally Non-Adherent and Contains Large Cracks, Permitting Atmospheric Exposure of UC_2 (U)

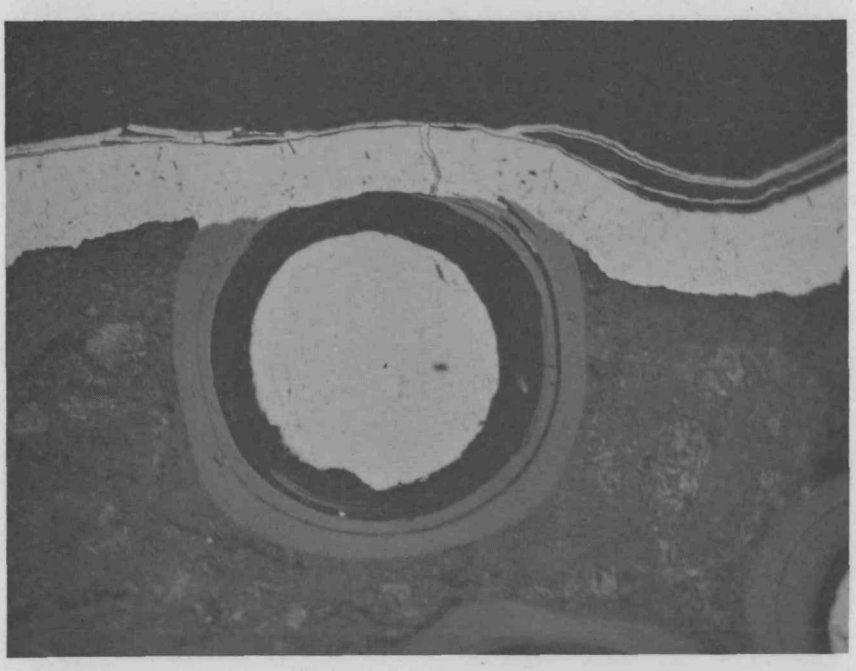

Figure 3-3B. (C) XE-2 Fuel Element Coating is Generally Adherent with Numerous Small Cracks in the Coating. The Small Cracks and the Surface of the Coating Are Overcoated with Mo which Further Reduces Access of Moisture to Exposed UC_2 (U)

Figure 3-3. (C) Comparison of Coating-Matrix Appearance of XE-1 and XE-2 Fuel Elements (U)

(C) Estimates have been made of the amount of UC_2 available for hydrolysis in a fuel element containing 125 grams of uranium. The machining operation would be expected to expose 600 to 900 fuel particles per inch of element bore. The leaching process (HCl at 1700°C for 3 hours) may be expected to remove more than 90 percent of this exposed UC_2. A diffusion controlled coating process used to form a 2-mil NbC coating would expose an additional 60 fuel particles per inch of element bore. Measurements of exposed UC_2 on coated fuel elements indicate that between 20 and 100 particles are exposed per inch of bore.

(C) Major sources of water within the XE-1 reactor are the graphite reflector which contains 1600 ppm of water and graphite fuel elements which contain 60 ppm of water. Taking into account the weight of the core and the reflector, approximately 600 grams of water are potentially available for the hydrolysis reaction. During the 3-1/2 month storage of the sealed XE-1 reactor, it is highly probable that the relative humidity within the reactor reached 100 percent. It is also likely that condensed water formed within the reactor.

(U) Experimental evidence obtained from all NERVA fuel element suppliers indicates that extensive hydrolysis generally does not occur in fuel elements stored at ambient conditions. This conclusion was obtained from detailed metallographic examination of fuel elements stored for periods of time up to 2 years. The apparent disagreement between this result and literature observations on rapid hydrolysis of bulk UC_2 at ambient conditions suggests that some passivating mechanism occurs with exposed fuel particles. Experimental studies reveal that the passivating mechanism can be made ineffective by treatment in acid (HCl or acetic) contaminated environments. Specific information is lacking on the passivating mechanism and the mechanism of sensitization of UC_2 particles by hydrolysis. One of the objectives of a continuing hydrolysis program is to provide a better understanding of these mechanisms.

(C) One potentially important factor in the sensitization effect relates to the availability of chloride contamination on fuel elements. Chemical analysis measurements show that

the fuel elements typically contain 1 to 5 ppm chloride ion. Assuming that most of this chloride contamination results from the NbC coating process (involving HCl and $NbCl_5$) and that it is concentrated on or near the NbC coating, the chloride ion contamination is 10 to 65 ppm of the NbC coating. Local regions of the element may contain extremely high concentrations of chloride ion. Thus, the fuel elements are contaminated with materials which may sensitize UC_2 fuel beads to hydrolysis.

3.4 LABORATORY HYDROLYSIS PROGRAM

(C) A laboratory hydrolysis program was initiated to provide experimental support for the proposal that hydrolysis caused the XE-1 debris. The laboratory program involved the exposure of samples of XE-1 fuel elements to various hydrolyzing environments of temperature ranging from ambient to 98°C. Some of the results of this program are presented with the aid of photographs. Figure 3-4 shows a variety of metallographic views of hydrolysis, including evidence of hydrolysis-related coating defects. Figure 3-5 illustrates the vehavior of external coatings when fuel particle hydrolysis occurs.

(C) The results of this investigation show rather conclusively that the hydrolysis reaction can cause the type of debris observed within the XE-1 reactor. Additional work is underway to both improve the understanding of the hydrolysis mechanism in XE-1 fuel elements and also to develop processes for the minimization and elimination of potential hydrolysis problems in NERVA fuel elements.

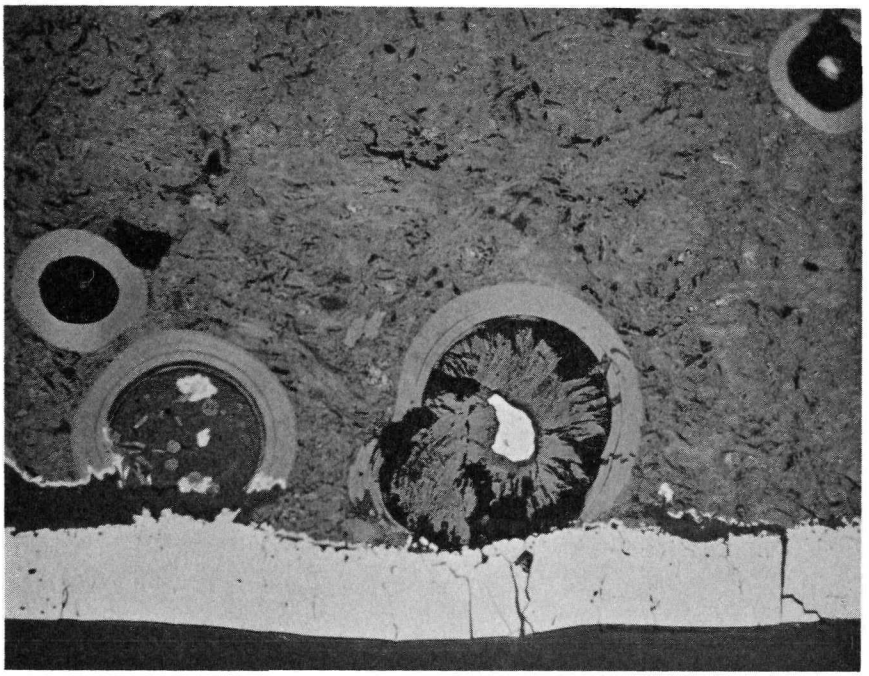

Figure 3-4A. (C) Hydrolysis Reaction Caused Cracking of Pyrocarbon Shell and Some Lifting of NbC Coating (C)

Figure 3-4. (C) Illustrations of the Effects of UC_2 Hydrolysis at the Coating-Substrate Interface Obtained in Laboratory Experiments (C)

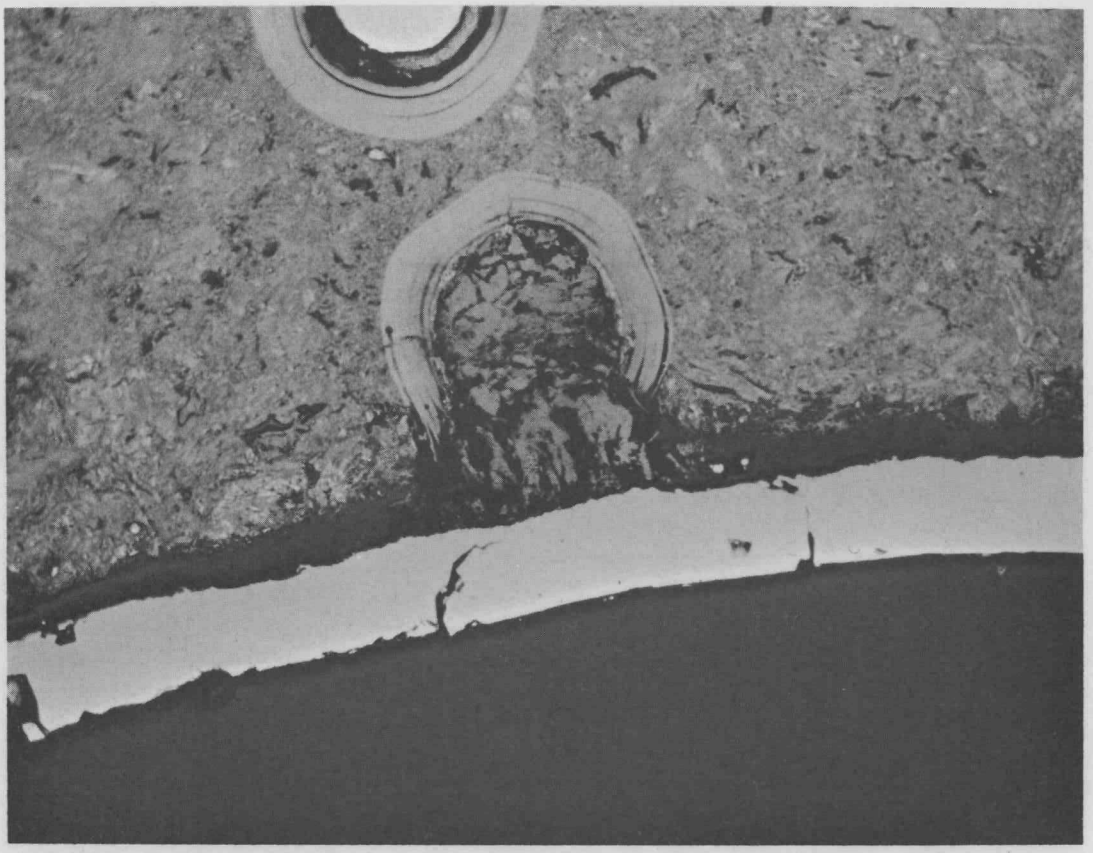

Figure 3-4B. (C) Hydrolysis Reaction Products Caused Further Separation and Cracking of NbC Coating (C)

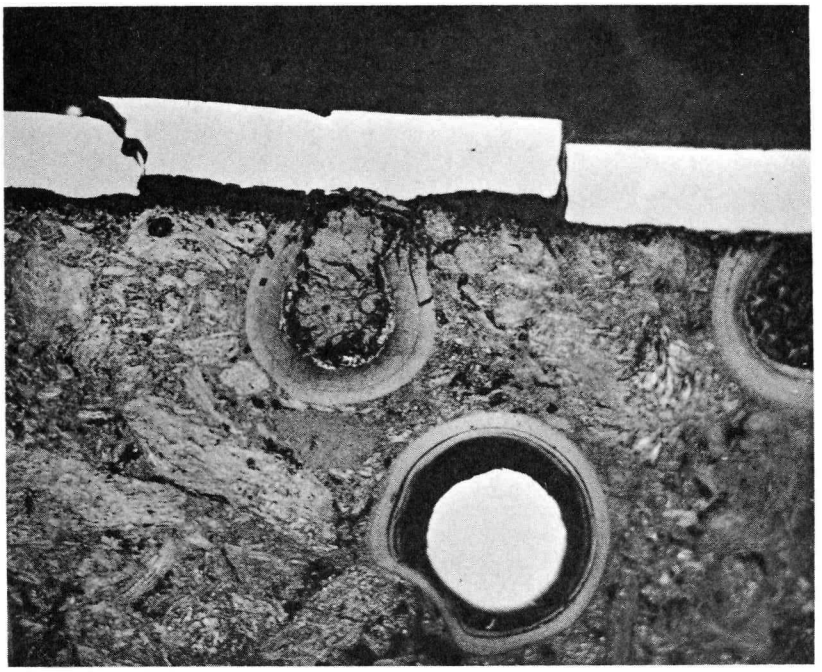

Figure 3-4C. (C) Illustration of the Formation of a NbC Coating Flake by UC_2 Hydrolysis (C)

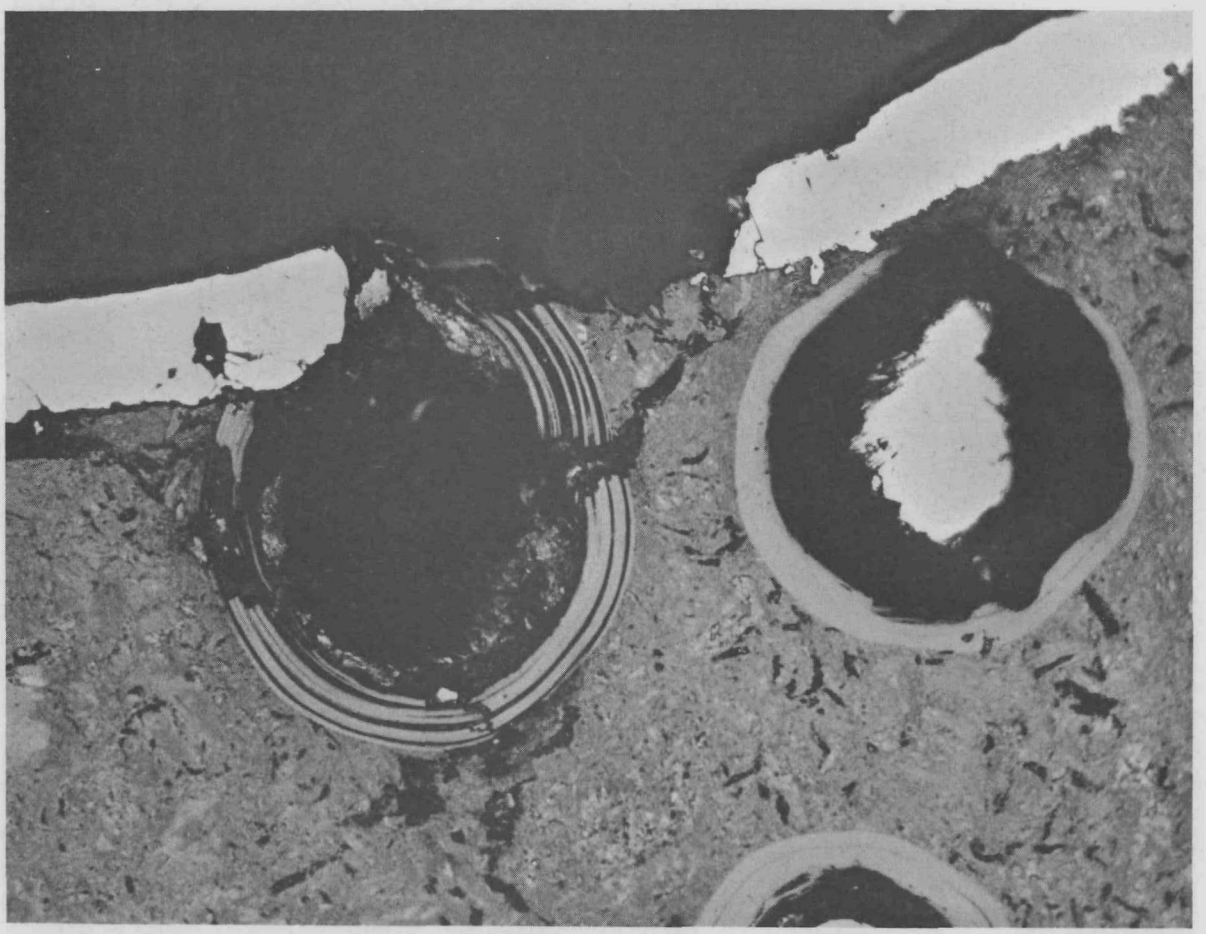

Figure 3-4D. (C) Loss of NbC Coating and Cracking of Fuel Matrix and Pyrocarbon Shell Caused by UC_2 Hydrolysis (C)

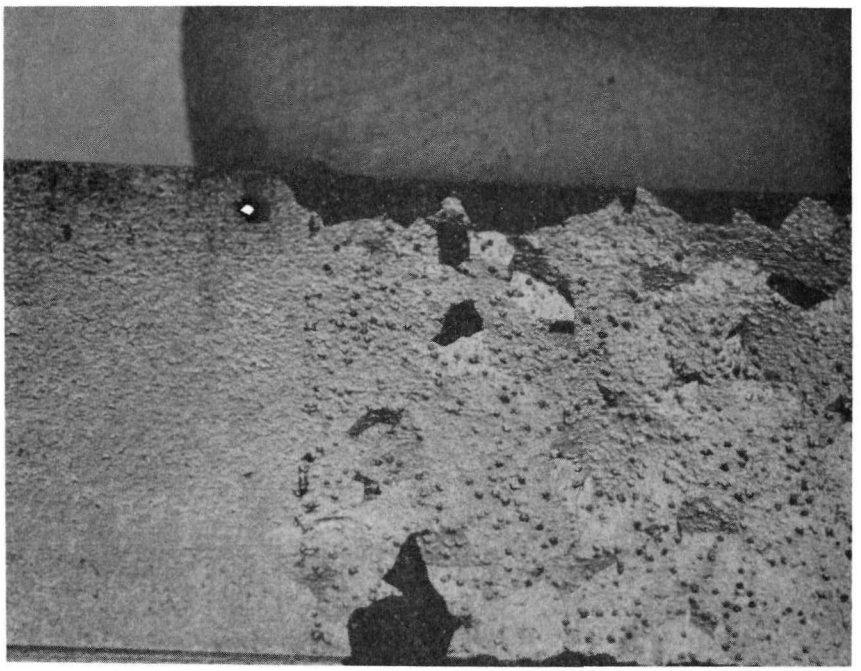

Figure 3-5. (C) NbC Flaking and Blistering on External Surface of Fuel Element Caused by Hydrolysis (C)

4.0 COMPOSITE MATERIALS*

4.1 INTRODUCTION

(C) The performance of niobium carbide coated graphite (ATJ) components in the NRX-reactors tested has demonstrated that the protection offered by the coating is marginal. Axial support system components (support blocks, washers, cups, etc.) have exhibited coating adherence loss after 30 minutes of reactor operation. The loss of adherence is apparent as either flaking of the coating or as a coarsening of the coating crack pattern generally referred to as crazing. Adherence loss and subsequent flaking is a result of (1) carbon diffusion from the substrate graphite-coating interface through the coating and (2) the mechanical forces developed as a result of the difference in the thermal expansion coefficients of the graphite and NbC (Table 4-1). In addition to the adherence problem, coated components are prone to chipping damage during inspection and reactor assembly.

4.2 DESCRIPTION OF GRAPHITE-CARBIDE COMPOSITES

(C) A class of materials consisting of a mixture of graphite and a carbide phase was developed, principally by LASL, to overcome the problems associated with NbC-coated graphite. The mixed powders (-150 + 325 meal graphite flour and 3 to 5 micron average Fisher subsieve size NbC powder) are consolidated into billet form by hot pressing at 3000°C and 3000 psi in graphite dies for times ranging from 10 to 60 minutes. Billet sizes of up to 3.5 inches in diameter by 4.5 inches long have been produced commercially. Densities of about 94 percent of theretical were attained, assuming 7.796 gm/cc for NbC and 2.26 gm/cc for the graphite.

(C) The material currently being evaluated for reactor application by WANL is the 75 weight percent NbC + graphite (47 volume percent NbC) composition. This composition was selected by a trade-off between thermal shock resistance and coating retention after corrosion testing. Compositions with higher carbide contents tend to fail due to thermal shock, while those of lower carbide content tend to exhibit inferior coating retention.

---

*L. L. France and R. H. Singleton

TABLE 4-1

(C) THERMAL EXPANSION OF SEVERAL MATERIALS (U)

Material	Orientation	CTE x 10^6 in/in/°C (16 to 2500°C)
75 w/o NbC Composite	AG	7.5
	WG	8.6
NbC (X-Ray Data)	Isotropic	7.2
ATJ	AG	5.9
	WG	4.4

4.3 PROPERTIES OF COMPOSITE MATERIALS

(C) The microstructure of an NbC coated 75 weight percent composite is shown in Figure 4-1. It is not readily apparent from this structure that the graphite and NbC are continuous interconnected phases. When the uncoated composite is corrosion tested in hydrogen, the graphite phase is removed, leaving a porous free-standing carbide structure. It would be predicted that this composition of approximately 50 volume percent NbC and the constituent powder sizes used could result in a structure of two continuous interconnected phases. This is verified by the corrosion experiment.

(C) The thermal expansion of the 75 weight percent NbC composite is approximately equal to that of NbC and, thus, crack-free and stree-free coatings are deposited. Samples with protective NbC coatings of from 1 to 2 mils thick have been corrosion tested in hydrogen for periods of up to 3 hours at 220°C without exhibiting any loss of coating. Some graphite is removed from the interface, but the continuous carbide phase of the composite substrate is adequate to retain the coating. The carbide phase of the composite is continuous with the NbC coating and acts as "roots" which aid in mechanically attaching the coating to the substrate.

(C) The corrosion rate, or rate of graphite removal from the uncoated composite, is approximately a factor of 10 lower than the rate of corrosion of unrooted graphite at 2200°C. Graphite is removed from the bare composite at a rate of about 0.7 mils/min, while the corrosion rate for bare graphite is between 7 and 10 mils/min. Thus, if the coated composite component is chipped or damaged during assembly or reactor operation, it is structually degraded at about one-tenth the rate of an equivalent chipped coated graphite component.

(C) The mechanical behavior of the 75 weight percent NbC composite is substantially different from that of either graphite or NbC. The compressive creep deformation of the composite is higher than higher graphite or NbC. Figure 4-2 shows the compressive test creep deformation after 1-hour for several temperatures and stress levels. The higher creep deformation of the 75 weight percent NbC composite makes it necessary that component design be compatible with some limited creep deformation.

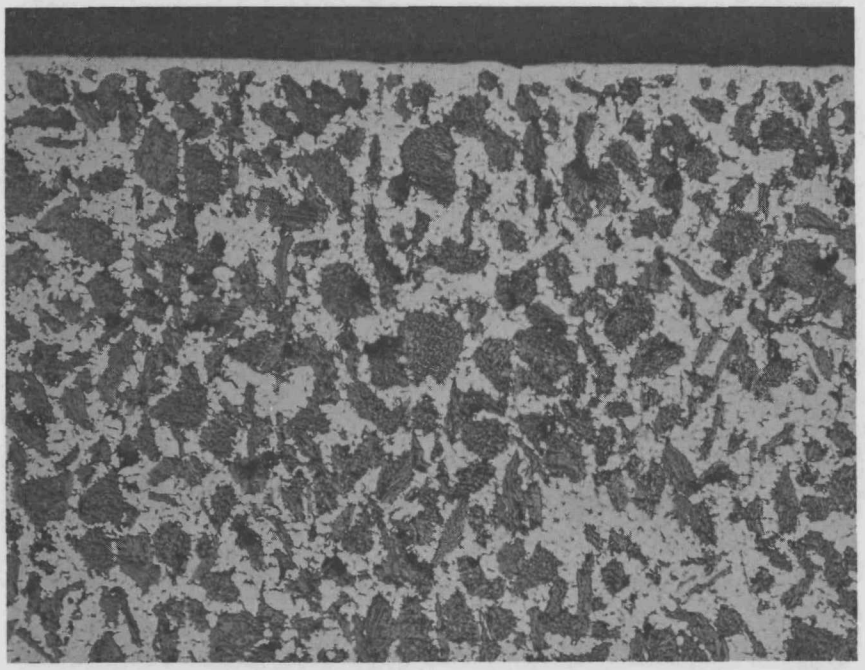

Figure 4-1. (C) Typical Microstructure of 75 w/o NbC Combonte with a 1 Mil Nbc Coating (100X) (C)

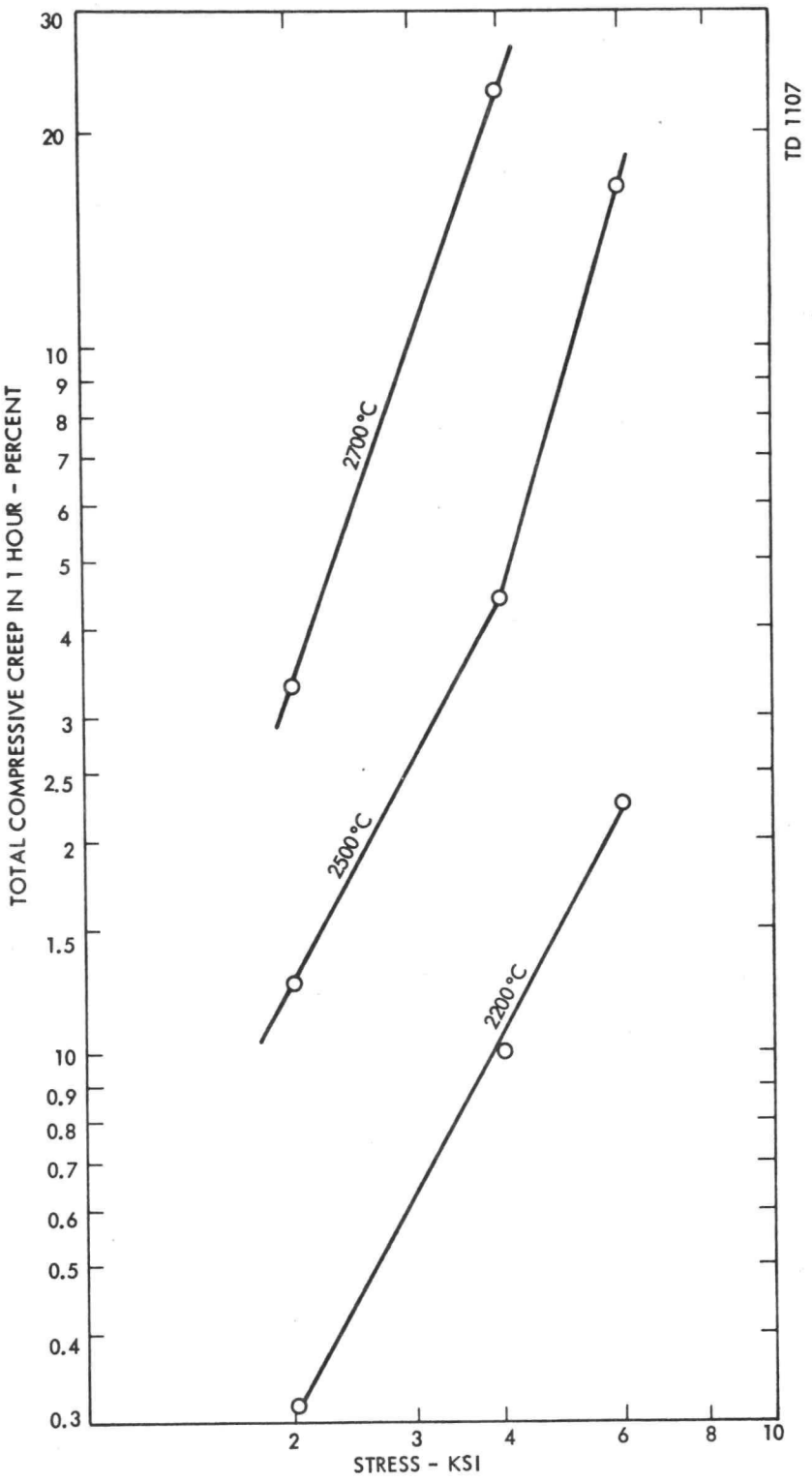

Figure 4-2. (C) Total Compressive Creep in 1 Hour of a 75 w/9 NbC-Graphite Composite, Across-Grain Orientation (C)

(U) The moduli of rupture (flexure strength) for several temperatures in both the with-grain (WG) and across-grain (AG) directions are shown in Figure 4-3. Based on the presently available data, this material does not show the strength increase with increasing test temperature which is typical of graphite.

(U) The Young's modulus of this composite is higher that that of graphite, being approximately 10×10^6 psi. This high modulus coupled with the higher thermal expansion substantially increases the sensitivity of this material to thermal stresses. This problem can be partially handled by design considerations and entails primarily the use of thin-wall sections to minimize the effect of rapid thermal transients.

(C) The 75 weight percent NbC composite, in general, is representative of a class of material which has unique characteristics with regard to retention of protective carbide coatings, but possesses mechanical and thermophysical properties which impose certain design limitations.

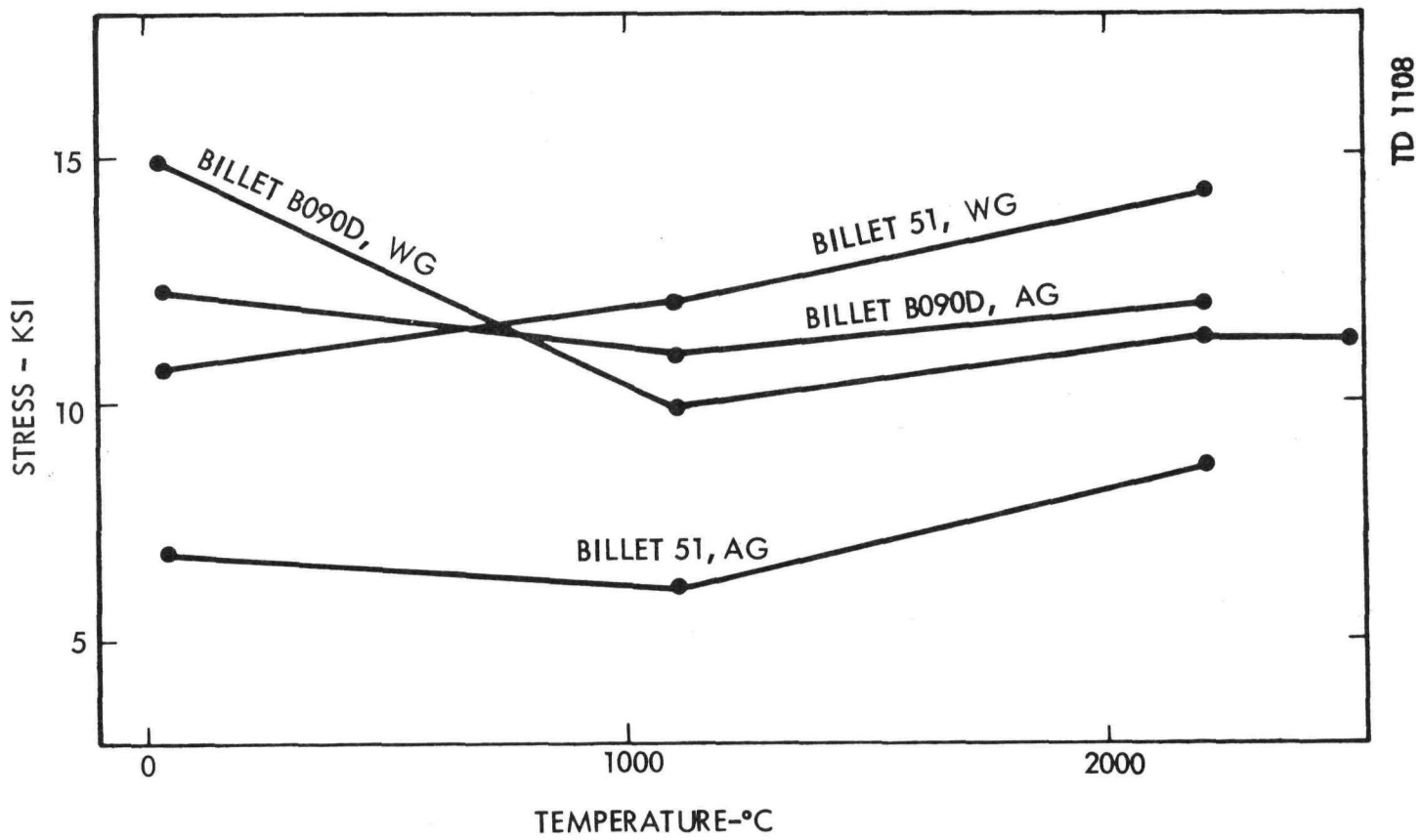

Figure 4-3. (C) Flexural Strengths of 75 w/o NbC-Graphite Composites as Functions of Temperature (C)

5.0 COMPRESSIVE CREEP BEHAVIOR OF THE GROUPS IV AND V REFRACTORY METAL MONOCARBIDE *

5.1 INTRODUCTION

(U) The creep behavior of the refractory metal monocarbides is presently being studied for the following purpose: (1) to establish a basis for the development of high carbide content composites, and (2) as a foundation for alloy carbide development. Specimens of theoretically dense carbides, of the order of 3/4-inch length by 3/8 inch diameter, have been prepared by carburizing the liquid metals into carbide rods. This method produces large-grained carbides with carbon-to-metal ratios near the maximum attainable.

5.2 CREEP DATA

(U) Samples were tested in compressive creep over the 1600 to 2700°C temperature range and 1000 to 4000 psi stress range. The total strains for a series of 1 hour creep tests and the minimum creep rates observed in these tests are plotted against test temperature in Figure 5-1. Note that HfC is the most creep resistant of the carbides studies.

(U) The high creep resistance is evidently related to the high yield stress, high melting point, and high activation energy for metal diffusion in the carbide. Vanadium monocarbide, in contrast, which has the highest creep rate, has the lowest yield stress, melting point, and activation energy. The yield stress of the carbides studies are plotted against temperature in Figure 5-2.

(U) The activation energy for creep was determined from the minimum creep rate at the end of 1 hour. The minimum creep rate appeared constant for approximately the last half-hour of the test and was taken to be the steady-state value. The activation energies determined are listed in Table 5-1. The activation energy, however, appears low when compared to either the activation energy for metal or carbon diffusion, thus suggesting a Pierls stress controlled mechanism. Measurements of the activation volume V* can determine whether a Pierls mechanism is controlling, since for a Pierls mechanism V* is usually 10 to 100 $\bar{b}^3$ and independent of strain. The activation volume as a function of temperature and strain was determined

*W. F. Brizes

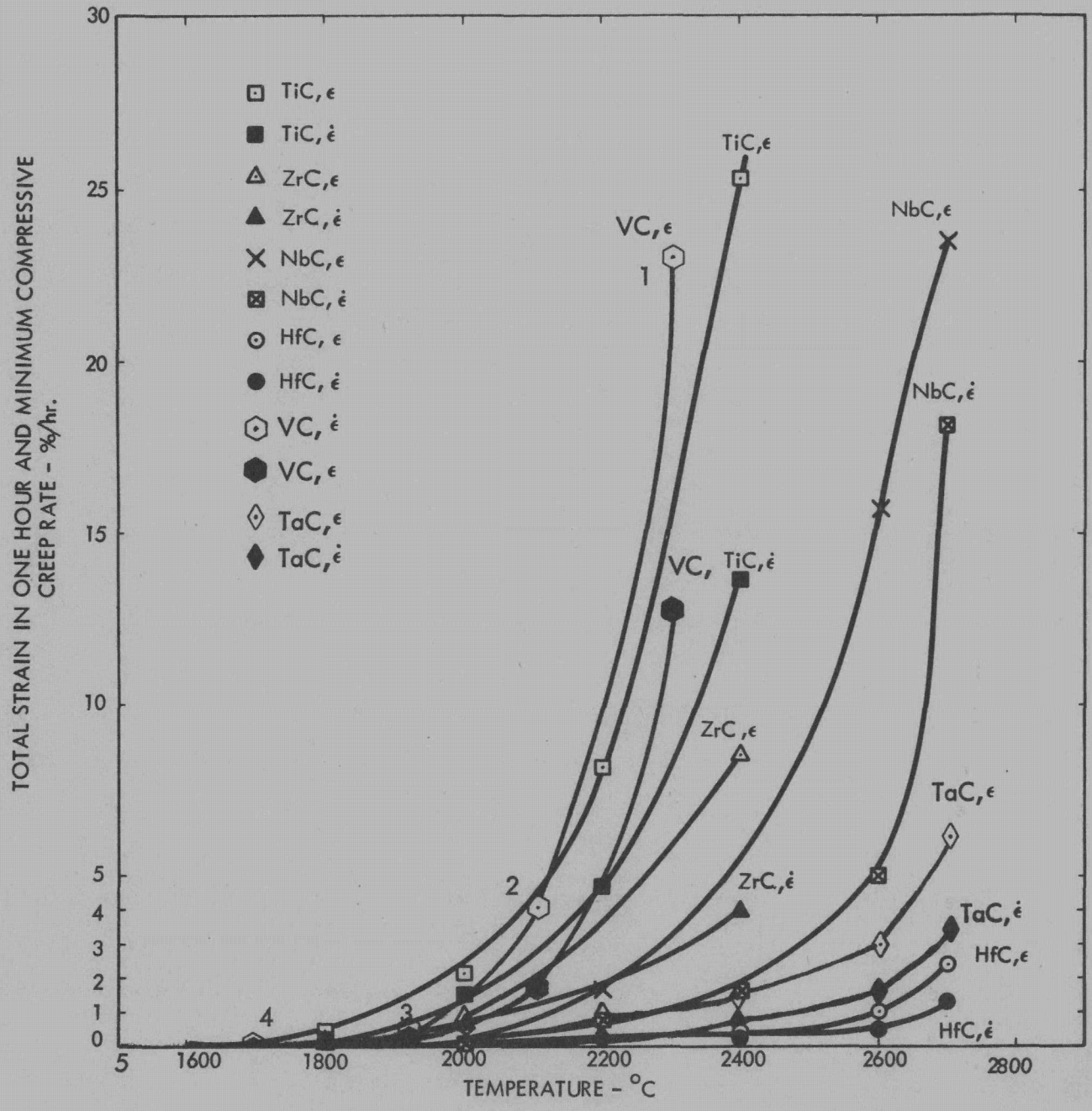

Figure 5-1. (U) Total Strain (E) and Minimum Compressive Creep Rate (E) after 1-Hour Test at 4000 psi Stress Versus Temperature for Group IVB and Group VB Monocarbides. (Vanadium Carbide Was Tested at 2000 psi Stress.) (U)

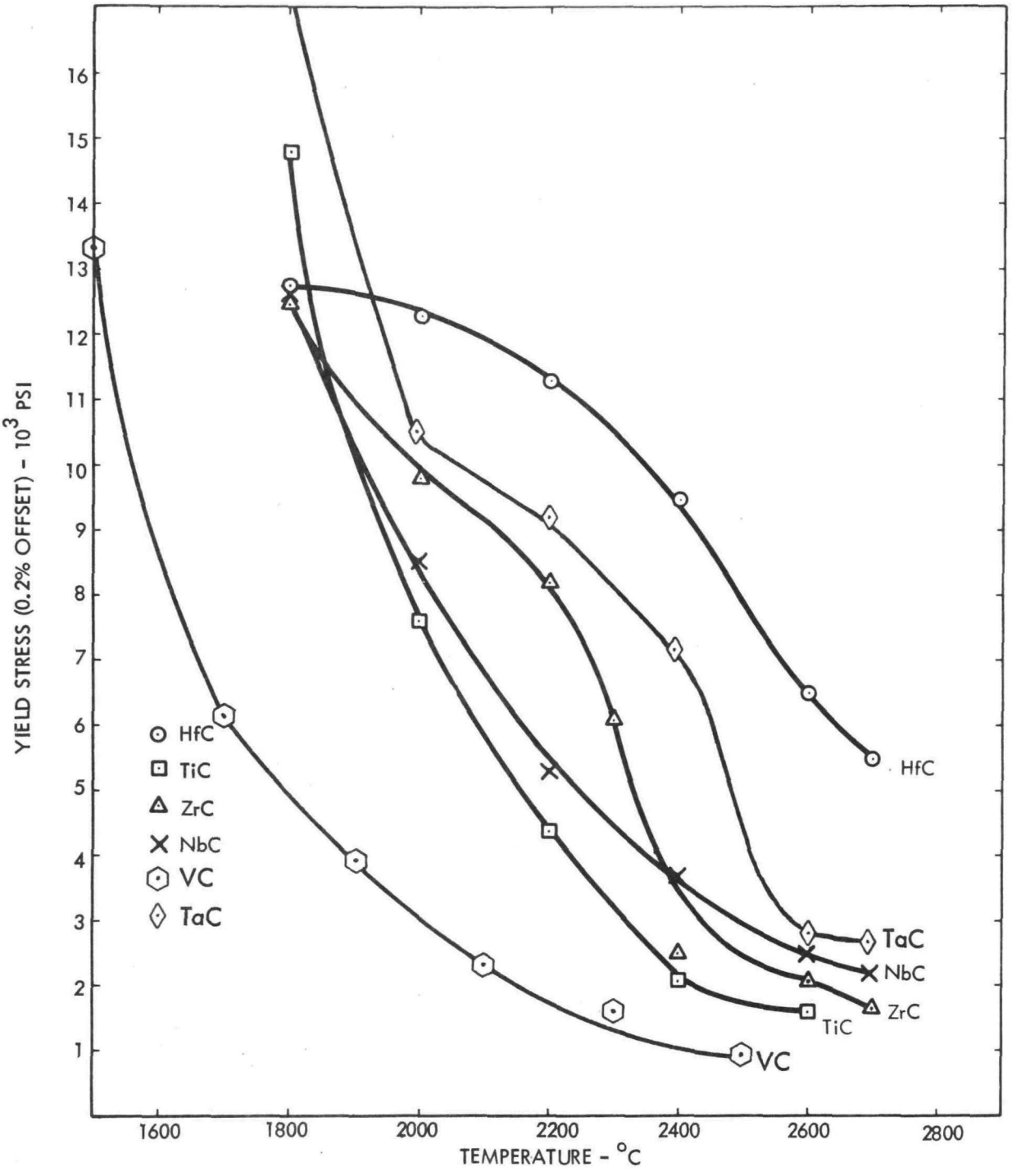

Figure 5-2. (U) Yield Stress for 0.2 Percent Offset Versus Temperature for Refractory Metal Monocarbides (U)

for each of the six monocarbides. It was found that V* was much larger than $100\,\bar{b}^3$ and dependent on strain, indicating that a Pierls mechanism is not controlling. However, at lower temperatures the activation volume does approach $100\,\bar{b}^3$ and shows little dependence on strain, indicating that a Pierls mechanism could control at lower temperature ($<0.5\,T_{mp}$). The activation volumes determined for TiC are given in Figure 5-3 and are typical of the other five monocarbides.

(U) The activation energy determined from the minimum creep rate is thus thought to be in error. Error could result from the structural dependence of the activation energy. This error is normally overcome by measuring the activation energy from instantanous temperature changes. Measurements on two of the carbides have been completed and are given in Table 5-1. The activation energies determined are higher than those determined from minimum creep rate and fall in the range intermediate between carbon and metal diffusion, indicating that a complex diffusion controlled mechanism may be operating at the higher temperatures.

5.3 HARDNESS DATA

(U) Hardness measurements were made across the compositional range of the monocarbides to determine if the strength of the Me-Me, Me-C, and C-C bonds varies with carbon vacancy concentration. The data, presented in Table 5-2, show variation in hardness. In the Group IV carbides the electronic contribution by the carbon atom increases the bonding as reflected by hardness measurements from 1700 KHN for $TiC_{0.54}$ to 3600 KHN for $TiC_{0.92}$. In the Group V monocarbides, bonding decreases with addition of carbon, i.e., from 3600 KHN for $TaC_{0.73}$ to 1850 KHN for $TaC_{0.98}$. Since bonding, diffusion, and yield strengths are interrelated, the creep deformation is expected to behave accordingly.

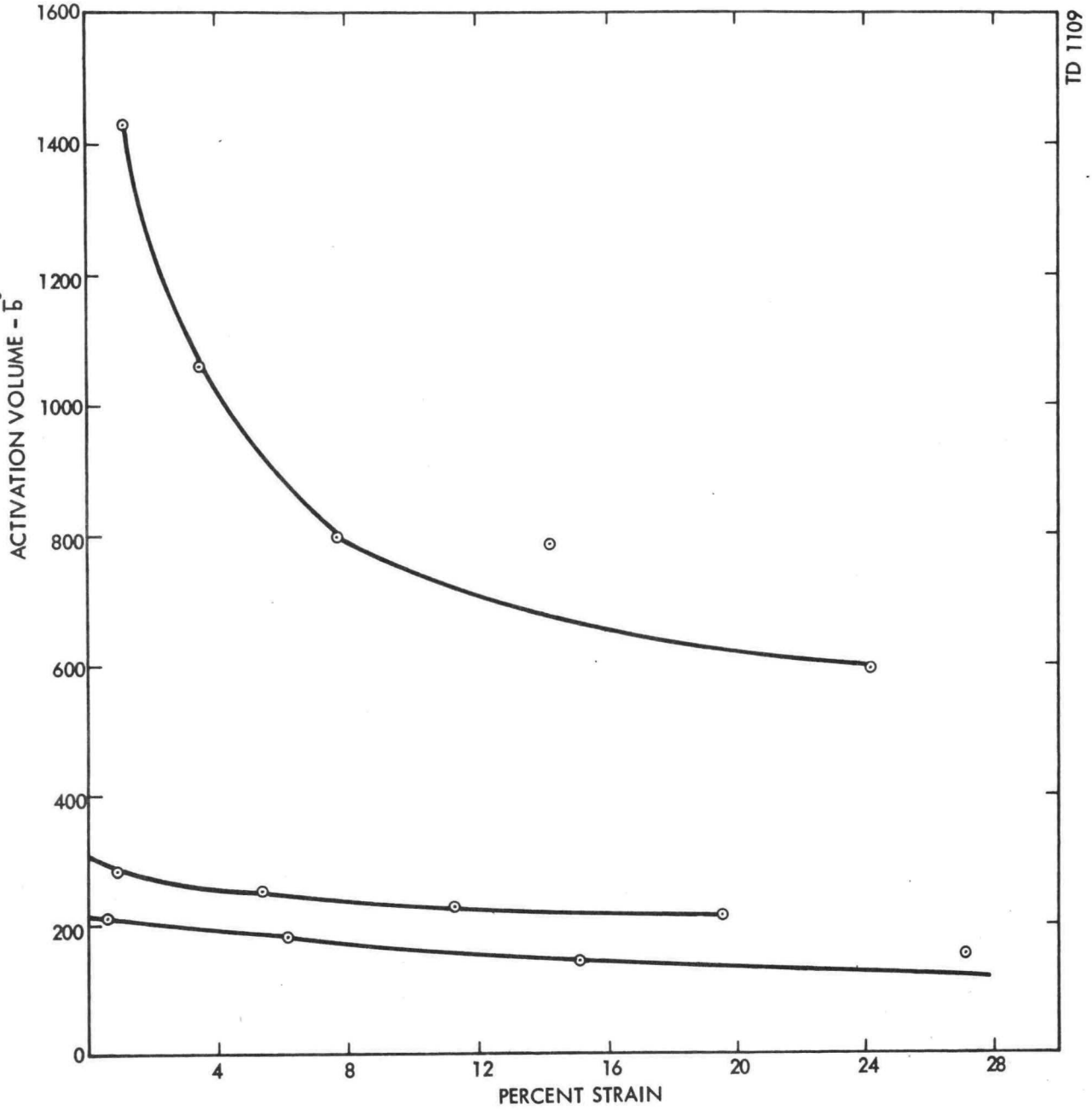

Figure 5-3. (U) Activation Volume of TiC as a Function of Strain (U)

TABLE 5-1

(U) ACTIVATION ENERGY FOR CREEP, CARBON, AND METAL DIFFUSION IN THE TRANSITION METAL CARBIDES (U)

	Q(K Cal/mole °K) (from minimum creep rate)	Q(K Cal/mole °K) (from instantaneous temperature changes)	Q^{C}_{MeC} (K Cal/mole °K) (from diffusion experiments)	Q^{Me}_{MeC} (K Cal/mole °K) $\left(Q^{Me}_{MeC} 38\ T_{mp}\right)$
TiC	76.4		58.7	120
ZrC	80.0	108	78.7	150
HfC	52.8		99.5	155
VC	121		55.2	85
NbC	56.5		88.2	130
TaC	61	91.7	89.6	142

TABLE 5-2

(U) RANGE OF HARDNESS FOR TRANSITION METAL MONOCARBIDES (U)

	KH		KH
$TiC_{0.92}$	3600	$VC_{0.82}$	2280
$TiC_{0.54}$	1700	$VC_{0.70}$	2370
$ZrC_{1.0}$	2550	$NbC_{1.0}$	1850
$ZrC_{0.61}$	1550	$NbC_{0.70}$	3550
$HfC_{0.92}$	2400	$TaC_{0.98}$	1850
$HfC_{0.61}$	1900	$TaC_{0.73}$	3600